small structures
www.small-structures.com

Edge Engineering in MoS_2 by Chemically Induced Nano-Folding

Edoardo Chini, Fiorenza Esposito, Vasiliki Benekou, Mohsin Muhyuddin, Eugenio Lunedei, Giampiero Ruani, Rita Rizzoli, Gabriele Calabrese, Fabiola Liscio, Franco Corticelli, Luca Seravalli, Pasquale D'Angelo, Vincenzo Palermo, Carlo Santoro, Andrea Candini, Denis Gentili,* and Massimiliano Cavallini**

This study introduces a straightforward technique for edge engineering in MoS_2 flakes through chemically induced nano-folding. By utilizing a buffered oxide etchant solution, precise detachment is achieved from the substrate and controlled folding/rolling of MoS_2 flakes, resulting in the creation of additional active edges up to 100 times thicker than the original flake. The model material, MoS_2 grown on silicon substrates via chemical vapor deposition, undergoes a dramatic transformation in morphology. This transformation is driven by partial detachment from the substrate, followed by bending and folding of the flake boundaries, which generates well-defined additional edges. The impact of edge thickening is demonstrated on fundamental characteristics such as work function, crystallinity, and catalytic properties. Notably, the findings demonstrate that the engineered edges significantly enhance the electrocatalytic activity of MoS_2 in hydrogen evolution reactions. This highlights the potential of this method to substantially improve the performance of low-dimensional materials.

1. Introduction

Boundaries and edges are some of the most diffuse defects in solid materials. Although often undesirable, these features play a crucial role in determining the properties and characteristics of materials.[1] Edges influence and can even generate a variety of physical and chemical properties, ranging from magnetism[2] to ion storage for batteries,[3] catalytic effects[4] and optical.[5] Edge properties primarily arise due to the intrinsic strain localized along these edges structures[6] and atoms located at the edge of a material experiencing translational symmetry breaking. These significantly alter electronic states at the edges due to local structural deformation, dangling, and unsaturated bonds, leading to electron confinement, boundary states, and edge polarization.[7] Therefore, exposing more edge sites is an effective strategy for probing the physical and chemical properties of a material, enhancing its electronic or catalytic functionalities, and exploring the applications in electronics, optoelectronics, catalysis, electrocatalysis, sensing, and quantum technologies.[8,1b]

Edges and boundaries are significant in the bulk phase but become critical in surfaces, thin films, and layered materials.[8,9] However, despite their crucial role, studying quantitatively the effects of edges on functional properties is challenging due to the difficulty of precisely controlling their size, thickness, and spatial distribution. Grain boundary[10] and edge[8] engineering

E. Chini, E. Lunedei, G. Ruani, R. Rizzoli, G. Calabrese, F. Liscio, F. Corticelli, D. Gentili, M. Cavallini
Istituto per lo Studio dei Materiali Nanostrutturati (ISMN)
Dipartimento di Scienze Chimiche e Tecnologie dei Materiali (DSCTM)
Consiglio Nazionale delle Ricerche (CNR)
Via P. Gobetti 101, 40129 Bologna, Italy
E-mail: denis.gentili@cnr.it; massimiliano.cavallini@cnr.it

F. Esposito, L. Seravalli, P. D'Angelo
Istituto dei Materiali per l'Elettronica ed il Magnetismo (IMEM)
Dipartimento di Ingegneria, ICT e Tecnologie per l'Energia e i Trasporti (DIITET), Consiglio Nazionale delle Ricerche (CNR)
Parco Area delle Scienze, 37/A, 43124 Parma, Italy

The ORCID identification number(s) for the author(s) of this article can be found under https://doi.org/10.1002/sstr.202500046.

DOI: 10.1002/sstr.202500046

F. Esposito
Department of Chemical Science
University of Parma
Life and Environmental Sustainability
43124 Parma, Italy

V. Benekou, V. Palermo, A. Candini
Istituto per la Sintesi Organica e la Fotoreattivita (ISOF)
Dipartimento di Scienze Chimiche e Tecnologie dei Materiali (DSCTM)
Consiglio Nazionale delle Ricerche
Via P. Gobetti 101, 40129 Bologna, Italy
E-mail: candini@isof.cnr.it

M. Muhyuddin, C. Santoro
Electrocatalysis and Bioelectrocatalysis Laboratory (EBLAB)
Department of Materials Science
University of Milano-Bicocca
Via Roberto Cozzi, 55, 20126 Milano, Italy

are the most successful strategies for studying and enhancing the properties of solids related to the edge effect. Principal approaches include: 1) Lithographic/patterning methods: Various conventional and unconventional methods have been proposed to fabricate artificial boundaries. These include photolithography,[11] electron beam lithography,[12] stamp-assisted electrochemistry[13] nanoimprinting,[14] scanning probe lithography,[15] laser irradiation,[16,1a] wet lithography[17] and spatially controlled phase segregation.[18] Although these methods are quite efficient, they require complex procedures or instrumentation. Moreover, they often introduce additional defects into the system; for example, ultraviolet or electron beam irradiation can create additional atomic defects in the basal plane of materials, compromising their stability.[19] 2) Edge/grain boundary engineering methods encompass growth,[8] confined template growth,[20] dewetting[21] and chemical etching methods.[22,1d] These processes were employed to fabricate nanoribbons, edges, and grain boundaries. However, despite their effectiveness, they restrict their applications to specific materials. Furthermore, the generated boundaries and edges are usually not quantified.

In this study, we report a straightforward approach for edge engineering based on controlled chemically induced nano-folding in transition metal dichalcogenides flakes. Specifically, we exploited the controlled detachment and rolling of MoS_2 flakes from surfaces, inducing a spatially limited nano-folding. Unlike other methods, our approach exploits a morphological reorganization in MoS_2 flakes, generating additional strained active edges and improving material properties without the need for any specific equipment.

We developed our method using MoS_2 as a model material because it is one of the most studied 2D transition metal dichalcogenides, in which the defects can generate and tailor[13] various properties. For example, it was recently shown that, in this material, edge defects and grain boundaries influence intrinsic doping, leading to the enhancement or inhibition of the trion formation.[23] For electrochemical reactions such as hydrogen evolution reactions (HERs), the activity primarily arises from the strained edges while the basal plane remains nearly inactive.[24,4a] The higher activity of the strained edge is linked to the optimization of hydrogen adsorption-free energy and the effect of unsaturated and dangling bonds facilitating the charge transfer.[25] Moreover, folded MoS_2 monolayers revealed intriguing optical and structural properties, such as a reduced interlayer coupling, with an enhancement of photoluminescence (PL) emission,[26] a significant blueshift of the A-exciton peak due to exciton screening[27] and novel phonon and exciton behaviors due to variations in the interfacial coupling in folded MoS_2 bilayers.[28]

The MoS_2 flakes were characterized using Optical Microscopy (OM), confocal micro-Raman Spectroscopy (μ-Raman), PL, Atomic Force Microscopy (AFM) and Kelvin-Probe Force Microscopy (KPFM). To evaluate the effects of edge enhancement on functionality, we investigated its effectiveness in catalyzing the Hydrogen Evolution Reaction in acid media, a critical application for MoS_2 in which edges are recognized as playing a determining role[4,22d] and considering its impact on several electrochemical reactions, such as hydrogen and oxygen evolution reactions.[29]

2. Results and Discussion

MoS_2 thin films were deposited on highly doped silicon substrates using Chemical Vapor Deposition (CVD),[30] employing liquid molybdenum precursors to grow high-quality flakes.[31]

We used two types of technologically relevant substrates: silicon with 280 nm of thermally grown SiO_2 (referred to as SiO_2/MoS_2) and silicon with native SiO_2 (referred to as Si/MoS_2).

SiO_2/MoS_2 samples. When grown Si with thermal SiO_2 on top (details in experimental), MoS_2 flakes predominantly exhibit regular, triangular shapes, covering ≈15%–20% of the substrate surface. Typically, the flake dimensions range from 30 to 100 μm in size and from 0.9 ± 0.2 to 1.9 ± 0.3 nm in thickness (**Figure 1**a), corresponding to 1 or 2 monolayers (MLs). OM (Figure 1a,b), PL (Figure S1, Supporting Information), and Raman spectroscopy (Figure 1c) confirm the high quality of the samples.

Si/MoS_2 samples. When grown on Si with native oxide (i.e. 1 nm thick) at high temperatures (820 °C), MoS_2 flakes grow embedded in a SiO_2 matrix, mainly 11 ± 3 nm deep (**Figure 2**a). The SiO_2 matrix forms by Si oxidation during the high-temperature stage of the process. Once the first layer of a flake is formed, Si oxidation beneath is inhibited, while Si oxidation between the flakes persists throughout the entire process. This process results in the growth of flakes embedded in the SiO_2 matrix (Figure 2a). A sketch of the process is shown in Figure S2, Supporting Information.

Unlike SiO_2/MoS_2, the flake dimensions in Si/MoS_2 samples range from 1 to 5 μm in size and from 0.9 ± 0.2 to 10 ± 1.1 nm in

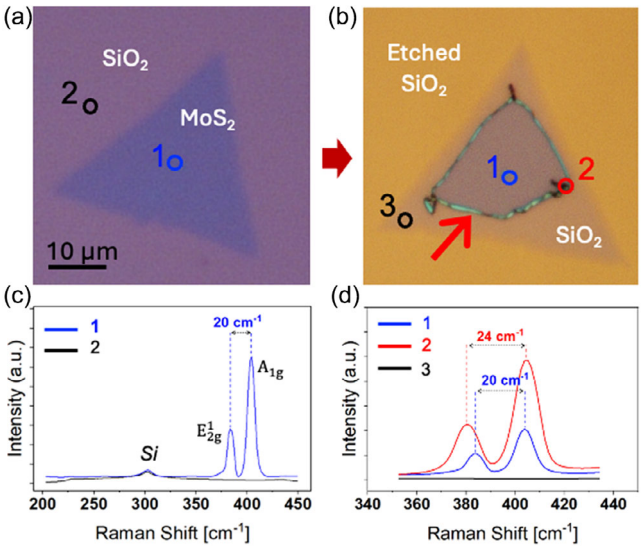

Figure 1. Optical image and Raman characterizations of MoS_2 flake deposited on thermal SiO_2 a) before and b) after BOE etching. The image shows the detachment of a flake by rolling (red arrow). The color change of the substrate is due to the reduction of SiO_2 thickness caused by HF etching. The contrast in correspondence of detached flakes (point 3) is due to the local difference in substrate thickness caused by the partial flakes' protection from HF action. c) Raman spectra acquired inside a pristine flake (position 1 in a) and in the substrate (position 2 in a). d) Comparison of Raman spectra recorded inside the partially detached flake (position 1 in b), the rolled zone (position 2 in b), and on the substrate at a position where the flake was present before detachment (position 3 in b).

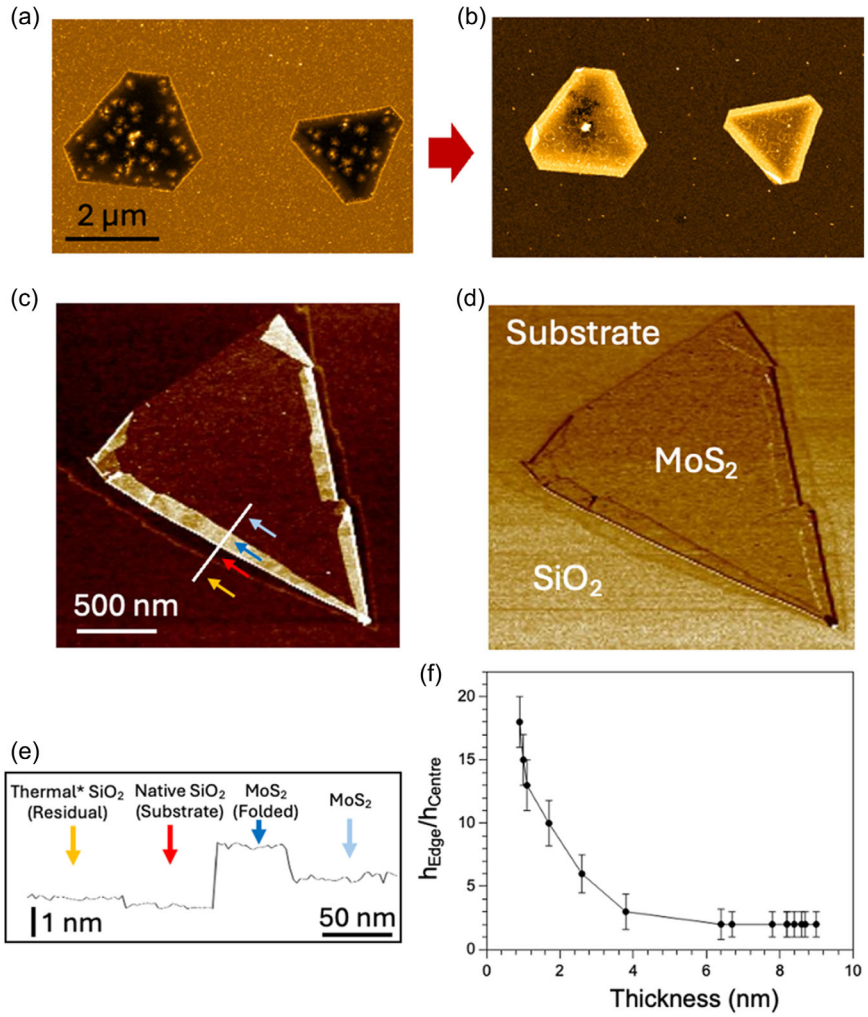

Figure 2. AFM characterization of MoS_2 flakes deposited on Si after BOE etching. a) Pristine sample. MoS_2 flakes are embedded in the SiO_2 matrix. b) Sample after etching. The image depicts the MoS_2 flake in relief. c) Detail of "b" showing MoS_2 nano-folding in a monolayer thick flake. This particular AFM image reveals a residual layer ≈0.6±0.2 nm thick of SiO_2 on the substrate, enabling us to illustrate the shape and size of the flake before a partial detachment. d) Corresponding phase image. e) The edges of the flake in "c" are twice as thick as its inner section. Moreover, their shape and size correspond perfectly to the imprint in the residual SiO_2 film surrounding the flakes, indicating edge nano-folding. f) Ratio between the edge and the center thickness (h_{Edge}/h_{Center}) plotted versus the h_{Center}, obtained by statistical analysis of 75 flakes in 10 AFM images.

thickness. Si/MoS_2 samples exhibited a markedly higher surface density of flakes than SiO_2/MoS_2 due to surface defects like dislocations and terrace boundaries on the Si surface, which act as nucleation sites.[32] The large variation in thickness is attributed to the confinement established by the SiO_2 matrix, which hampers the lateral growth of the flakes and favors the formation of thicker flakes. Moreover, embedded flakes often exhibit an irregular distribution of nanometric grains, attributed to products of the chemical reactions occurring during MoS_2 formation.[31a]

2.1. Edges Engineering in MoS_2 by Chemically-Induced Bending plus Folding in Large Flakes

The MoS_2 thin films were treated with buffered oxide etchant (BOE), a solution of HF/NH_4F commonly used in microelectronics to etch thermal-SiO_2 at a controlled rate, typically in the range 30−80 nm min^{-1}. When applied to SiO_2/MoS_2 samples, BOE action combines the etching of HF on SiO_2 with the intercalation capacity and detachment effects of NH_4^+.[33] While surface treatments over 10 s remove all flakes completely, shorter treatments (e.g., 5 s) significantly altered the morphology of the flakes. Specifically, upon short BOE treatment, the flakes began to detach from the edges. Flakes smaller than 20 μm (indicative value) were completely removed from the substrate and could not be observed on the substrate anymore; larger flakes were instead only partially detached, forming thicker edges. The tick of flake edges (zone 2 in Figure 1b) ranges from 60 to 100 nm (i.e., till more than 100 times thicker than the flake). Figure 1 shows optical images of a SiO_2/MoS_2 sample before and after the short BOE treatment, illustrating the partial detachment of flakes.

We investigated the nature of thickened edges by μ-Raman spectroscopy, a recognized technique for probing crystallinity, occurrence, and the types of defects in MoS_2. The MoS_2 Raman spectrum displays two distinctive peaks centered at 385 cm^{-1} (A_{1g}), corresponding to in-plane and out-of-plane vibrations. The broadness and variation in the position of these bands depend on the number of layers (from 19 cm^{-1} for one monolayer to 24 cm^{-1} for more than five layers and bulk), built-in strain, and the quality of the flakes (i.e., crystallinity, occurrence/type of defects).[34]

μ-Raman spectrum recorded inside the flake (position 1 in Figure 1a) shows the characteristic E^1_{2g} and A_{1g} peaks, shifted by 19–20 cm^{-1} (Figure 1c). This value is compatible with 1-2 MLs thicknesses, considering the built-in strain in MoS_2 flakes grown by liquid precursors can affect the Raman spectra.[31b] Importantly, the spectrum of MoS_2 measured at the center of the flake is not affected by the BOE treatment (Figure 1d), and no peaks related to atomic defect formation appear at other frequencies (Figure 1c). This evidence suggests that, unlike treatment by highly concentrated HF,[35] the mild concentration of HF in the BOE solution does not damage the MoS_2 crystalline structure in our experimental condition.[36] In contrast, spectra recorded at the edge of detached flake zones (position 2 in Figure 1b) show a significant increase in the Raman signal and a shift of 24 cm^{-1} (i.e., equal to bulk), corresponding to possibly thicker flakes and to edges straining. Notably, although the forms of pristine flakes remain visible under the optical microscope after the short BOE treatment, no Raman signal was detected in the areas where they appear detached (position 3 in Figure 1b). We explained this effect on the basis that the optical contrast of the flakes arises from interference phenomena associated with the thickness of MoS_2. During the etching treatment, before the MoS_2 flakes begin to detach, they shield the substrate from HF etching, resulting in a thicker layer of SiO_2 that replicates the original shape of the pristine flake. This variation in SiO_2 thickness, shaped by the pristine flake, produces the contrast observed under OM after detachment (details in Section 2.3).

2.2. Edges Engineering in MoS_2 by Chemically-Induced Bending plus Nano-Folding in Small Flakes

The detachment of flakes has been utilized as a straightforward technique for edge engineering in MoS_2 flakes. To this aim, we applied the BOE treatment to MoS_2 flakes embedded within a thin layer of SiO_2, produced by growing MoS_2 directly on Si substrates. BOE treatment up to 3 s removed only partially the SiO_2, leaving the flakes still partially embedded in the SiO_2 matrix. BOE treatment for 5 s completely removed the SiO_2 matrix, causing the flakes to emerge as relief structures (Figure 2b). Emerged flakes displayed various thicknesses, ranging from 0.9 ± 0.2 nm, corresponding to one monolayer (ML), to 10 ± 1.1 nm (multiple layers). Importantly, over 95% of flakes display clearly defined edges whose widths range from 50 to 100 nm and are 2 to 18 times thicker than their inner part (Figure 2d). Moreover, their lateral size is systematically 100–200 nm smaller than the pristine flakes (Figure 2c and S4, Supporting Information). AFM maps sensitive to the surface chemical composition, such as adhesion and phase images, do not show significant differences between the inner zone and the edges (Figure 2d).

Figure 2c shows a high-resolution AFM image of a sample treated for 5 s with BOE solution, in which a residual layer of SiO_2, measuring 0.6 ± 0.2 nm thick, is still present on the surface (indicated by the yellow point in Figure 2c). Although this residual SiO_2 layer is not consistently observed in AFM images, this detail offers crucial insights into the mechanism of edge thickening. The edges of the flake are twice as thick as the inner part (1.9 ± 0.3 and 0.9 ± 0.2 nm, represented by the blue and light-blue points in Figure 2c). Furthermore, their shape and size perfectly correspond to the imprint left in the residual SiO_2 film surrounding the flakes (marked by the red point in Figure 2c). This nearly perfect alignment between the thicker areas and the lateral empty space clearly indicates that, as a result of the BOE treatment, the edges of the flakes fold toward the inner region (Note: We consider as "folding" when the bent layer is parallel to the flake's surface (Figure 4a). We consider as "Rolling" when, after multiple foldings, the bent layers start to be curved (Figure 4b)).

Using statistical analysis, we correlated the thickness of folded edges and the thickness of unfolded central areas of MoS_2. Figure 2f shows the trend of the ratio between the edge and the center thickness (h_{Edge}/h_{Center}) versus the h_{Center}, obtained by analyzing 75 flakes in 10 AFM images. Notably, while flakes thicker than 3 MLs increase the edge thickness by one or two times, flakes 1 or 2 MLs thick can increase it by up to 18 times.

We have further investigated the nature and properties of the enhanced edges by μ-Raman spectroscopy and KPFM.

While the Raman spectrum recorded inside the flakes remains almost unaltered upon the short BOE treatment, the spectra recorded at the edge were consistently more intense in the treated samples (**Figure 3**d and S4d, Supporting Information). In addition, the separation between A_{1g} and E^1_{2g} peaks is systematically higher at the edges from 1 to 4 cm^{-1}, suggesting that the edges might be made of a multilayer of MoS_2 thicker than the center (Figure 2c).

KPFM allows the microscopic mapping of the surface's electrical potential (SP), which is related to the difference in work functions between the sample and the AFM probe.[37] Figure 3 shows a BOE-treated flake's topography and the corresponding SP image of a MoS_2 flake one ML thick (0.9 ± 0.2 nm). The topographic image (Figure 3a) clearly shows an increase in thickness at the edge, which is 1.9 ± 0.3 nm, corresponding to a bilayer. The SP image (Figure 3b) reveals a strong contrast between the flake and the substrate (Si with native SiO_2). This image accurately reproduces the flake shape and shows a variation in SP of -90 ± 8 mV in the center of the flake (corresponding to a work function of 5.2 eV), while, at the edge, the SP further decreases to -106 ± 10 eV. In our experimental configuration, this change corresponds to an increase in the work function of the thicker part of the MoS_2 flake. This behavior perfectly aligns with theoretically predicted energy changes related to the number of MoS_2 layers and previous experimental KPFM investigations.[38]

2.3. Mechanism of the Process

A "bending plus folding/rolling" mechanism would explain the big differences in the thickness between the areas at the flakes' perimeter and the flakes' center.

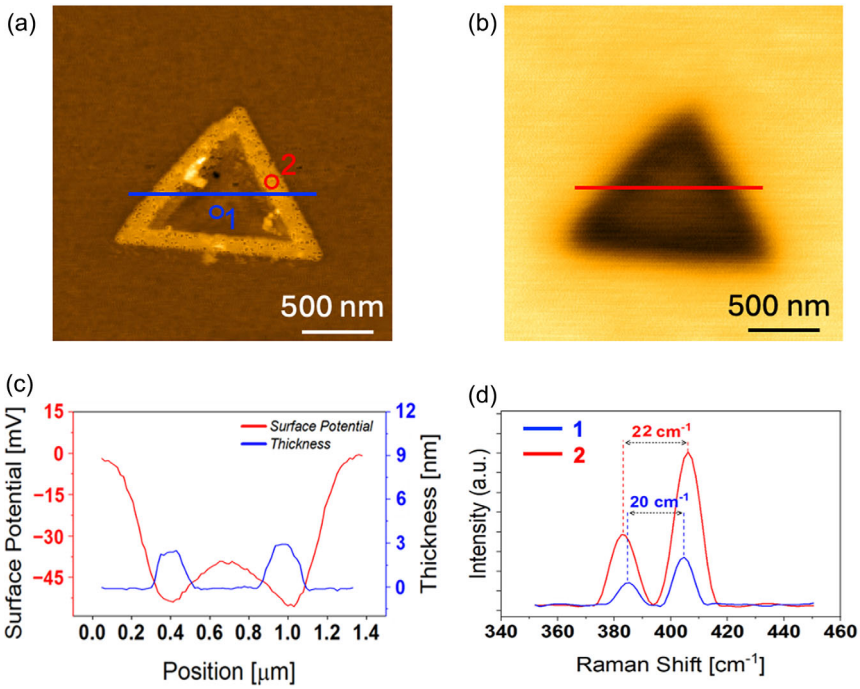

Figure 3. Topographic and electronic characterization of BOE treated Si/MoS_2 flakes. a) AFM topographic image. b) Surface potential image. A lower potential value (higher WF) suggests the formation of a multilayer at the edges. c) Topographic (blue line) and surface potential profile (red line) of a,b images. d) Raman spectra of MoS_2 films as collected on the center of a flake (blue line) and at the edge (red line) ($\lambda_{exc} = 514$ nm).

In SiO_2/MoS2 samples, both the etching action of HF and the detaching action of NH4+ occur during the entire process (i.e., for 5s). HF etches the SiO_2, reducing its thickness in the regions between the flakes, which causes the contrast observed with the optical microscope; simultaneously, the action of NH_4^+, a known agent largely used for MoS_2 exfoliation,[39] induces the detachment of flakes of several microns. The intercalation of NH_4^+ is well-established and discussed elsewhere.[39] Because of the low thickness of the flakes (1-2 ML), which have low bending stiffness, the detached flakes' edges can easily bend toward the inner part and successively fold upon layer–layer van der Waals interactions, forming the multilayer at the edges. Multiple reiterations of this process can evolve in rolling, generating giant edges that can be >100 times thicker than the center of the flakes (Figure 1b). The resulting morphology of this case can be described as flake rolling, whose proposed mechanism is sketched in **Figure 4**a.

In contrast, in Si/MoS_2 samples, when flakes are embedded in the SiO_2 matrix, only the basal plane of the flakes is exposed to the BOE solution; thus, the detachment action of NH_4^+ is avoided until the overgrown SiO_2 layer is almost fully removed upon the etching action of HF on SiO_2 (Figure 4b). In these conditions, the flake detachment from the substrate occurs only in the final step of the process, and it is limited to only a few hundred nanometers. These conditions allow a limited number of folding reiterations, thus resulting in a reduced edge thickening, that is, <20 times with respect to the center (unembedded) of the flakes (Figure 2f).

Even if conventional mechanics cannot be applied to nanometric Van der Waals materials, experiments and modeling[1c] have demonstrated that the bending stiffness (D) of multi-layered flakes increases with the number of layers N as $D \approx N^{\alpha}$, with an exponent ranging from $\alpha = 1$ for poorly interacting sheets to $\alpha = 3$ for strongly adhering ones. Thus, thicker flakes are inhibited from repeated folding due to their greater rigidity, while thin layers can undergo multiple bending-rolling steps (Figure 4). Consequently, thin MoS_2 flakes on SiO_2 will have a larger edge-to-center thickness ratio, while thick flakes on Si will have a smaller thickness ratio.

2.4. Correlation Between Engineered Edge and Electrocatalytic Activity

To evaluate the functionalities of our engineered edges, we tested their effectiveness in catalyzing the HER in acid media for Si/MoS_2 samples. Although we are aware that our system is probably the worst possible configuration for catalysis (e.g., a 2D system with an inactive basal plane[24b] and suboptimal electrical contact between MoS_2 flakes and substrate), we chose this functionality as the electrocatalytic activity of MoS_2 is primarily generated by the defects at the edges.[4a,24b] We evaluated the electrocatalytic performance of MoS_2/Si samples before and after short BOE treatment by analyzing the linear sweep voltammetry (LSV) curves.

Pristine samples and samples exposed to BOE treatment for less than 3 s (i.e., with the flakes still embedded in the SiO_2 matrix, exposing only the basal plane to solution) are almost catalytically inactive (**Figure 5**, red curve), also if compared to conventional MoS_2 flakes.[4] This evidence, combined with

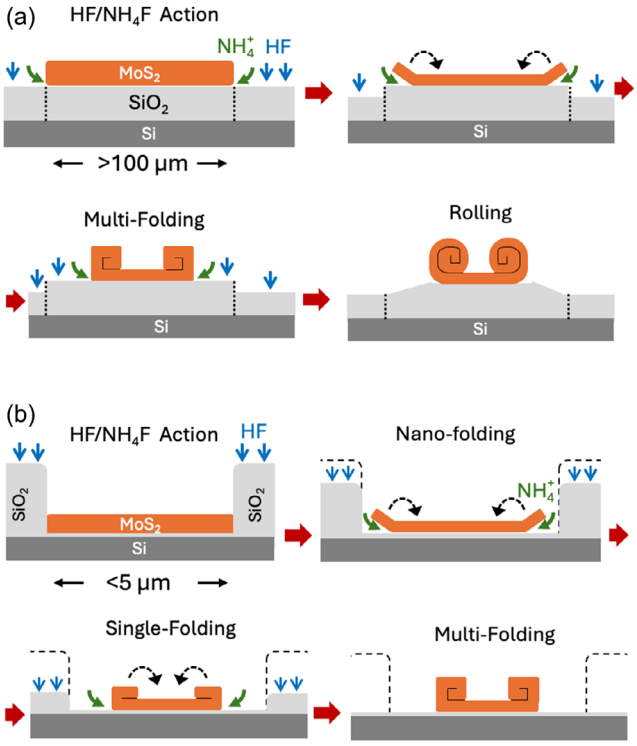

Figure 4. Schematic of the Process. a) In SiO_2/MoS_2 samples, the etching action of HF and the dethatching action of NH_4^+ occur throughout the entire process, leading to significant flake detachment. Dashed lines show the boundaries of pristine flakes. The different SiO_2 thickness generated by the initial protective action of the flake on SiO_2 is the cause of the optical contrast observed in Figure 1b. BOE treatment results in multiple bending and folding iterations, creating much thicker edges (up to 100 times thicker than the center of the flake). b) In Si/MoS_2 samples, the BOE treatment initially etches the thermal SiO_2. In the final step, nano-folding is induced, increasing the edge thickness. This folding can be repeated for thinner, less rigid flakes, resulting in thicker flakes, with a minimum thickness increase of 20 times.

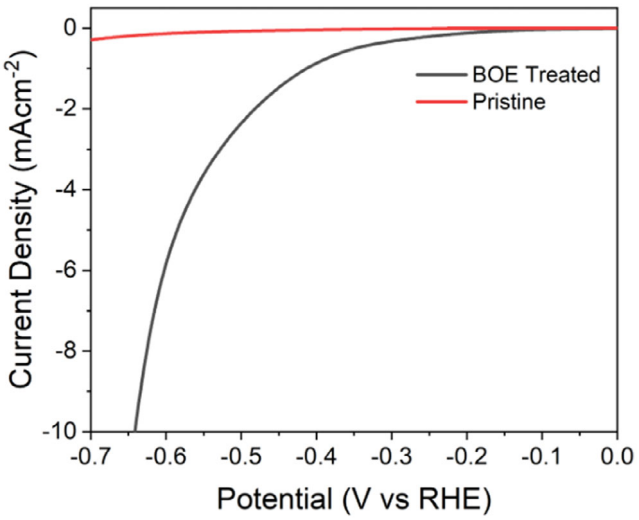

Figure 5. HER activity of the MoS_2 flakes in 0.5 M H_2SO_4 (N_2-purged). LSVs were acquired at a scan rate of 5 mV s^{-1}, assuming that the edges cover 2.7% of the total surface of the electrode. Pristine samples (which exclusively expose the basal plane, red curve) are catalytically inactive. Samples treated with BOE solution (black curve), which expose thickened edges, demonstrate a high current density, corresponding to an overpotential of −0.65 V versus RHE at a current density of 10 mA cm^{-2} (further details in "Experimental").

µ-Raman characterization, confirms that, under our experimental conditions, a short BOE treatment does not affect the properties of the basal plane, nor does it create detectable active atomic defects. Differently, longer BOE treatments (>5 s) yield samples exhibiting a higher electrocatalytic activity (Figure 5, black curve). Despite the suboptimal configuration of our system, the LSV curves demonstrate significant HER electrocatalytic activity in the BOE-treated samples, with an overpotential of approximately −0.64 V at a current density of 10 mA cm^{-2}.

The 5s BOE treatment removes the embedding and produces thicker, larger edges that serve as electrocatalytic sites. This evidence, along with the fact that the basal plane is electrocatalytically inactive, leads us to attribute the catalytic activity solely to the edges generated by the BOE treatment. The LSV curves reported in Figure 5 were measured considering the surface area of the edges determined from AFM topographic images. This measurement accounted for the fact that folded edges are thicker than the plane of the flake. Specifically, we selected the edges by applying a threshold of 1 nm in the high-resolution AFM topographic images, resulting in 2.7% of the total area (details in the experimental section).

The catalytic activity in HER of transition metal dichalcogenides strongly depends on the presence of highly strained regions.[40] Density functional theory (DFT) calculations showed that strain enhances the density of states near the Fermi level, decreasing the Gibbs free energy for hydrogen adsorption on the MoS_2 and thus facilitating hydrogen binding.[41] It was demonstrated that MoS_2 nanosheets undergoing macroscopic mechanical strain showed significantly steeper polarization curves and lower Tafel slopes than the unstrained ones,[42] which aligns with our measurements.

3. Conclusions

In conclusion, this study presents a straightforward method for edge engineering in MoS_2 flakes, focusing on enhancing both edge size and thickness through chemically induced nano-folding. The strain at the edges, resulting from the multi-folding of MoS_2 flakes, significantly affects the physical and functional properties of the material.

Our comprehensive analytical techniques and evaluations of chemical functionality confirm the effectiveness of this procedure in producing functional edges. We demonstrated that the functionalities of MoS_2 arise exclusively from artificial edge formation, especially in relation to its electrocatalytic properties for the HER.

This research represents a significant contribution to the field of defect and edge engineering in MoS_2, emphasizing the critical role of edge manipulation in advancing scientific and

technological research. The capacity to tailor material properties through edge engineering is vital for various applications, including electronics, 2-D devices, catalysis, and optoelectronics. Although MoS_2 flakes were utilized as model materials in this study, the methodology can be easily extended to other layered transition metal dichalcogenides. Overall, this work provides a robust strategy for manipulating material properties, thereby paving the way for new innovations in materials science.

4. Experimental Section

Materials: Sulfur powder (300 mg, 99.98%) was used as the sulfur precursor. The molybdenum precursor solution was prepared by mixing solutions of $(NH_4)_6Mo_7O_{24}{\cdot}4\,H_2O$, 99.99% (AHT), NaOH (growth promoter), and OptiPrep (a viscosity-increasing agent containing 60% iodixanol in water) in a volume ratio of 4:1:0.5, respectively. The NaOH solution had a concentration of 0.0625 M, while the AHT solution was 0.003 M, with both solutions prepared in ultrapure water. As BOE, we used a commercial solution of HF/NH_4F 7:1 solution of NH_4F:HF.

Substrates: 1) Highly doped silicon with a $<100>$ crystal orientation and a resistivity of 1–30 Ω·cm with a native SiO_2 layer, ≈1 nm thick (MoS_2/Si); 2) Highly doped silicon with a 280 nm thick thermally grown SiO_2 layer (MoS_2/SiO_2).

Before deposition, the substrates were cleaned in an ultrasonic bath using acetone (10′), isopropanol (10′), and ultrapure water (5′), followed by drying with nitrogen gas. Subsequently, they were treated with plasma generated from a mixture of O_2 (75%) and Ar (25%) at 25 W and 1 kg cm^{-3} for 5 min.

Sample Preparation: MoS_2 flakes were grown by CVD in an open quartz tube at 820 °C (in the reacting zone). The molybdenum precursor solution was spin-coated onto a 2 cm^2 substrate (40 µL, 4000 rpm, 40 s). The sulfur precursor, placed in an alumina boat, was independently heated at 160 °C in a separate temperature zone, positioned 20 cm away from the silicon substrate. The growth process occurred at atmospheric pressure in an inert atmosphere, using 6 N purity nitrogen as the carrier gas at a flow rate of 200 cm^3 min^{-1} for 10 min. This process resulted in high-quality MoS_2 flakes on the whole surface of the sample, displaying various shapes such as triangular, hexagonal, and more complex structures depending on the substrate used.

BOE Treatment: The samples containing MoS_2 flakes were treated with BOE solution, previously diluted in H_2O (1:1). The substrates were gently immersed horizontally in the solution for a few seconds (≈5 s) and subsequently rinsed thoroughly with ultrapure H_2O (via immersion) to stop the etching process. Afterwards, the samples were dried using a low-pressure, constant nitrogen flow for about 30 s.

Electrocatalysis: The HER activity of MoS_2 flakes was electrochemically evaluated using a three-electrode configuration. The working electrode comprised MoS_2 flakes deposited on a silicon substrate, mounted onto a copper plate using InGa. The total surface area of the working electrode was 0.125 cm^2. We assumed as an active area, the surface occupied by the BOE generated edges consisting of 2.7% of the total area (detail of its measure in *Measure of the edge surface area section*). A standard reversible hydrogen electrode (RHE, HydroFlex) was used as the reference electrode, while a titanium wire served as the counter electrode. Figure S6, Supporting Information, show a scheme of our electrochemical cell.

The electrocatalytic activity was analyzed in 0.5 M H_2SO_4 electrolyte. N_2 was purged through the electrolyte for 15 min before starting the measurements to remove oxygen from the solution. During the measurements, the potential range was maintained between 0 and −0.8 V versus RHE. A scan rate of 5 mV s^{-1} was used to record the HER polarization curves. The HER overpotential was determined at a current density of −10 mA cm^{-2}.

OM: Optical images were recorded with a Nikon i-80 microscope through a X20 objective lens. The images were recorded using a commercial CCD camera (Nikon CCD DS-2Mv).

Confocal µ-Raman Spectroscopy: µ-Raman spectra were recorded in backscattering geometry using a commercial (Renishaw) Raman microscope using the 532 nm Nd-YAG laser line through a X100 objective lens, achieving a spatial resolution of better than 0.5 µm under confocal conditions to measure the different zones of the flakes carefully.

AFM and Kelvin Probe Force Microscopy: AFM and KPFM imaging were obtained by a Multimode 8 microscope equipped with a Nanoscope V controller and type J piezoelectric scanner (Bruker, USA). Topographic images were obtained in "PeakForce" mode using ScanAsyst-Air probes in air at room temperature. KPFM images were obtained in, "Surface potential mode, a two-passage lift mode (lift height of 20–50 nm, without significant difference in the potential signal).[37] The images were analyzed using the open software Gwyddion for image analysis.[43] The presented images were lebeled by a first-order line and optimized in z-scale; no further filters were applied.

Measure of the Edge Surface Area: The area of the generated edges was measured from AFM topographic images, considering that folded edges were thicker than the plane of the flake. Specifically, we selected the edge by applying a threshold of 1 nm in the high AFM topographic images. The images were analyzed using the open software Gwyddion for image analysis.[43] Figure S5, Supporting Information, shows a representative example of the selected area.

Supporting Information

Supporting Information is available from the Wiley Online Library or from the author.

Acknowledgements

We thank the European Union for funded this research—Next Generation EU from the Italian Ministry of University and Research. project PRIN 2022SRHPF2 "Molecular assisted atom vacancies arrangement to modulate magnetism in 2D transition metal dichalcogenides" (MAVAM) and Italian Ministry of Environment and Energy Security POR H2 AdP MMES/ENEA with involvement of CNR and RSE, PNRR – Mission 2, Component 2, Investment 3.5 "Ricerca e sviluppo sull'idrogeno" under the ENEA – UNIMIB and ENEA-CNR agreements (Procedure 1.1.3 PNRR POR H_2). D. G. acknowledges support from the CNR via Progetti di Ricerca@CNR (NOENDCAT). L.S and F.E. acknowledge funding by MUR within the PRIN2022 project "2DIntegratE" (2022RHRZN2). We wish to acknowledge the help of Dr. Giovanni Attolini and Dr. Matteo Bosi in carrying out the CVD growth of MoS_2 flakes.

Conflict of Interest

The authors declare no conflict of interest.

Author Contributions

Edoardo Chini: formal analysis (lead); methodology (lead); writing—review and editing (supporting). **Fiorenza Esposito**: investigation (equal); methodology (equal). **Vasiliki Benekou**: investigation (lead); writing—review and editing (supporting). **Mohsin Muhyuddin**: investigation (equal); writing—review and editing (supporting). **Eugenio Lunedei**: investigation (supporting). **giampiero ruani**: investigation (lead); writing—review and editing (supporting). **Rita Rizzoli**: investigation (lead); writing—review and editing (equal). **Gabriele Calabrese**: methodology (supporting); writing—review and editing (supporting). **Fabiola Liscio**: supervision (lead); writing—review and editing (supporting). **Franco Corticelli**: investigation (supporting). **Luca Seravalli**: supervision (lead); validation (supporting); writing—review and editing (equal). **Pasquale D'Angelo**: investigation (supporting); supervision (supporting); writing—review and editing (supporting). **Vincenzo Palermo**: conceptualization (supporting); methodology (equal); supervision (lead); validation (equal); writing—review and editing (equal). **Carlo Santoro**: methodology (equal);

supervision (lead); writing—review and editing (supporting). **Andrea Candini**: methodology (equal); supervision (lead); writing—review and editing (equal). **Denis Gentili**: investigation (equal); methodology (lead); validation (lead); writing—review and editing (equal). **Massimiliano Cavallini**: conceptualization (lead); data curation (equal); formal analysis (equal); supervision (lead); writing—original draft (lead); writing—review and editing (lead).

Data Availability Statement

The data that support the findings of this study are available from the corresponding author upon reasonable request.

Keywords

edge engineering, MoS_2 flakes, nano-foldings

Received: January 23, 2025
Revised: March 24, 2025
Published online:

[1] a) S.-T. M. Akkanen, J. C. Arias-Muñoz, A. V. Emelianov, K. K. Mentel, J. V. Tammela, M. Partanen, S. Das, A. Faisal, M. Pettersson, Z. Sun, *Adv. Funct. Mater.* **2024**, *34*, 2406942; b) T. X. Huang, X. Cong, S. S. Wu, K. Q. Lin, X. Yao, Y. H. He, J. B. Wu, Y. F. Bao, S. C. Huang, X. Wang, P. H. Tan, B. Ren, *Nat. Commun.* **2019**, *10*, 5544; c) G. Wang, Z. Dai, J. Xiao, S. Feng, C. Weng, L. Liu, Z. Xu, R. Huang, Z. Zhang, *Physical Rev. Lett.* **2019**, *123*, 116101; d) R. Canton-Vitoria, T. Hotta, M. Xue, S. Zhang, R. Kitaura, *JACS Au.* **2023**, *3*, 775.

[2] G. Kondo, N. Yokoyama, S. Yamada, Y. Hashimoto, C. Ohata, S. Katsumoto, J. Haruyama, *AIP Adv.* **2017**, *7*, 125019.

[3] a) X. Jin, T. Lee, A. Soon, S.-J. Hwang, *Adv. Funct. Mater.* **2024**, *34*, 2316446; b) M. F. Niu, F. L. Wan, W. L. Xin, L. Zhang, X. L. Xiao, H. Zhang, Z. C. Yan, Z. Q. Zhu, *Batteries Supercaps* **2024**, *8*, e202400419.

[4] a) M. Muhyuddin, G. Tseberlidis, M. Acciarri, O. Lori, M. D'Arienzo, M. Cavallini, P. Atanassov, L. Elbaz, A. Lavacchi, C. Santoro, *J. Energy Chem.* **2023**, *87*, 256; b) J. Xie, H. Zhang, S. Li, R. Wang, X. Sun, M. Zhou, J. Zhou, X. W. Lou, Y. Xie, *Adv. Mater.* **2013**, *25*, 5807.

[5] J. Wang, Z. Wu, C. Yang, G. Chen, M. Yuan, B. Li, Y. Lai, R. Che, *Adv. Funct. Mater.* **2024**, *34*, 2409923.

[6] M. Tinoco, L. Maduro, M. Masaki, E. Okunishi, S. Conesa-Boj, *Nano Lett.* **2017**, *17*, 7021.

[7] a) Z. Lin, B. R. Carvalho, E. Kahn, R. Lv, R. Rao, H. Terrones, M. A. Pimenta, M. Terrones, *2D Mater.* **2016**, *3*, 022002; b) S. Zhou, J. Han, J. Sun, D. J. Srolovitz, *2D Mater.* **2017**, *4*, 025080.

[8] W. Fu, M. John, T. D. Maddumapatabandi, F. Bussolotti, Y. S. Yau, M. Lin, K. E. Johnson Goh, *ACS Nano* **2023**, *17*, 16348.

[9] T. Chowdhury, E. C. Sadler, T. J. Kempa, *Chem. Rev.* **2020**, *120*, 12563.

[10] T. Watanabe, *J. Mater. Sci.* **2011**, *46*, 4095.

[11] H. Kwon, S. Garg, J. H. Park, Y. Jeong, S. Yu, S. M. Kim, P. Kung, S. Im, *npj 2D Mater. Appl.* **2019**, *3*, 9.

[12] M. S. M. Saifullah, M. Asbahi, M. Binti-Kamran Kiyani, S. S. Liow, S. Bin Dolmanan, A. M. Yong, E. A. H. Ong, A. Ibn Saifullah, H. R. Tan, N. Dwivedi, T. Dutta, R. Ganesan, S. Valiyaveettil, K. S. L. Chong, S. Tripathy, *ACS Appl. Mater. Interfaces* **2020**, *12*, 16772.

[13] D. Gentili, G. Calabrese, E. Lunedei, F. Borgatti, S. A. Mirshokraee, V. Benekou, G. Tseberlidis, A. Mezzi, F. Liscio, A. Candini, G. Ruani, V. Palermo, F. Maccherozzi, M. Acciarri, E. Berretti, C. Santoro, A. Lavacchi, M. Cavallini, *Small Methods* **2024**, *9*, 2401486.

[14] C. C. Cedeno, J. Seekamp, A. P. Kam, T. Hoffmann, S. Zankovych, C. M. S. Torres, C. Menozzi, M. Cavallini, M. Murgia, G. Ruani, F. Biscarini, M. Behl, R. Zentel, J. Ahopelto, *Microelectron. Eng.* **2002**, *61–62*, 25.

[15] S. Chen, S. Kim, W. Chen, J. Yuan, R. Bashir, J. Lou, A. M. van der Zande, W. P. King, *Nano Lett.* **2019**, *19*, 2092.

[16] a) K. Vasu, S. S. R. K. C. Yamijala, A. Zak, K. Gopalakrishnan, S. K. Pati, C. N. R. Rao, *Small* **2015**, *11*, 3916; b) X. Wang, B. Wang, Q. Zhang, Y. Sun, E. Wang, H. Luo, Y. Wu, L. Gu, H. Li, K. Liu, *Adv. Mater.* **2021**, *33*, 2102435; c) J. Liang, W. Huang, Z. Zhang, X. Li, P. Lu, W. Li, M. Liu, Y. Huangfu, R. Song, R. Wu, B. Li, Z. Lin, L. Chai, X. Duan, J. Li, *Adv. Funct. Mater.* **2024**, *34*, 2407636.

[17] a) D. Gentili, P. Sonar, F. Liscio, T. Cramer, L. Ferlauto, F. Leonardi, S. Milita, A. Dodabalapur, M. Cavallini, *Nano Lett.* **2013**, *13*, 3643; b) M. Melucci, M. Zambianchi, L. Favaretto, V. Palermo, E. Treossi, M. Montalti, S. Bonacchi, M. Cavallini, *Chem. Commun.* **2011**, *47*, 1689; c) Y.-H. Hung, A.-Y. Lu, Y.-H. Chang, J.-K. Huang, J.-K. Chang, L.-J. Li, C.-Y. Su, *ACS Appl. Mater. Interfaces* **2016**, *8*, 20993.

[18] M. Cavallini, J. Gomez-Segura, C. Albonetti, D. Ruiz-Molina, J. Veciana, F. Biscarini, *J. Phys. Chem. B* **2006**, *110*, 11607.

[19] M. Cavallini, D. Gentili, *ChemPlusChem* **2022**, *87*, e202100562.

[20] J. Guo, L. Zhai, X. Zhang, J. Sheng, R. Qiao, K. Liu, Z. Xu, Y. Li, *Adv. Funct. Mater.* **2025**, *35*, 2408703.

[21] a) D. Gentili, G. Foschi, F. Valle, M. Cavallini, F. Biscarini, *Chem. Soc. Rev.* **2012**, *41*, 4430; b) M. Cavallini, R. Lazzaroni, R. Zamboni, F. Biscarini, D. Timpel, F. Zerbetto, G. J. Clarkson, D. A. Leigh, *J. Phys. Chem. B* **2001**, *105*, 10826.

[22] a) R. Ionescu, A. George, I. Ruiz, Z. Favors, Z. Mutlu, C. Liu, K. Ahmed, R. Wu, J. S. Jeong, L. Zavala, K. A. Mkhoyan, M. Ozkan, C. S. Ozkan, *Chem. Commun.* **2014**, *50*, 11226; b) J. Hu, B. Huang, C. Zhang, Z. Wang, Y. An, D. Zhou, H. Lin, M. K. H. Leung, S. Yang, *Energy Environ. Sci.* **2017**, *10*, 593; c) X. Hai, K. Chang, H. Pang, M. Li, P. Li, H. Liu, L. Shi, J. Ye, *J. Am. Chem. Soc.* **2016**, *138*, 14962; d) J. Kibsgaard, Z. Chen, B. N. Reinecke, T. F. Jaramillo, *Nat. Mater.* **2012**, *11*, 963.

[23] S. Golovynskyi, O. I. Datsenko, A. I. Pérez-Jiménez, A. Kuklin, M. Chaigneau, A. Golovynskyi, I. Golovynska, M. Bosi, L. Seravalli, *ACS Appl. Nano Mater.* **2024**, *7*, 15570.

[24] a) J. Zhu, Z.-C. Wang, H. Dai, Q. Wang, R. Yang, H. Yu, M. Liao, J. Zhang, W. Chen, Z. Wei, N. Li, L. Du, D. Shi, W. Wang, L. Zhang, Y. Jiang, G. Zhang, *Nat. Commun.* **2019**, *10*, 1348. b) J. Zhang, J. Wu, H. Guo, W. Chen, J. Yuan, U. Martinez, G. Gupta, A. Mohite, P. M. Ajayan, J. Lou, *Adv. Mater.* **2017**, *29*, 1701955.

[25] a) Y. Yin, J. Han, Y. Zhang, X. Zhang, P. Xu, Q. Yuan, L. Samad, X. Wang, Y. Wang, Z. Zhang, P. Zhang, X. Cao, B. Song, S. Jin, *J. Am. Chem. Soc.* **2016**, *138*, 7965. b) C. Tsai, F. Abild-Pedersen, J. K. Nørskov, *Nano Lett.* **2014**, *14*, 1381.

[26] A. Castellanos-Gomez, H. S. J. van der Zant, G. A. Steele, *Nano Res.* **2014**, *7*, 572.

[27] F. J. Crowne, M. Amani, A. G. Birdwell, M. L. Chin, T. P. O'Regan, S. Najmaei, Z. Liu, P. M. Ajayan, J. Lou, M. Dubey, *Phys. Rev. B* **2013**, *88*, 235302.

[28] Y. Liu, S. Wang, X. Chen, M. Yang, X. Li, B. Liang, *Opt. Mater.* **2021**, *111*, 110641.

[29] a) Y. Luo, L. Tang, U. Khan, Q. Yu, H.-M. Cheng, X. Zou, B. Liu, *Nat. Commun.* **2019**, *10*, 269; b) C. Zhang, Y. Luo, J. Tan, Q. Yu, F. Yang, Z. Zhang, L. Yang, H.-M. Cheng, B. Liu, *Nat. Commun.* **2020**, *11*, 3724.

[30] S. Y. Yang, G. W. Shim, S. B. Seo, S. Y. Choi, *Nano Res.* **2017**, *10*, 255.
[31] a) F. Esposito, M. Bosi, G. Attolini, F. Rossi, S. E. Panasci, P. Fiorenza, F. Giannazzo, F. Fabbri, L. Seravalli, *Appl. Surf. Sci.* **2023**, *639*, 158230; b) L. Seravalli, F. Esposito, M. Bosi, L. Aversa, G. Trevisi, R. Verucchi, L. Lazzarini, F. Rossi, F. Fabbri, *Nanoscale* **2023**, *15*, 14669.
[32] a) P. Leclere, M. Surin, R. Lazzaroni, A. F. M. Kilbinger, O. Henze, P. Jonkheijm, F. Biscarini, M. Cavallini, W. J. Feast, E. W. Meijer, A. Schenning, *J. Mater. Chem.* **2004**, *14*, 1959; b) V. Corradini, C. Menozzi, M. Cavallini, F. Biscarini, M. G. Betti, C. Mariani, *Surf. Sci.* **2003**, *532*, 249.
[33] a) J. Huang, T. Meng, F. Yi, Z. Cui, D. Shu, A. Gao, *J. Solid State Chem.* **2024**, *338*, 124837; b) W. Hu, H. Liu, W. Dong, H. Akif Munir, X. Fan, X. Tian, L. Pang, *J. Electroanal. Chem.* **2023**, *949*, 117882.
[34] a) S. Mignuzzi, A. J. Pollard, N. Bonini, B. Brennan, I. S. Gilmore, M. A. Pimenta, D. Richards, D. Roy, *Phys. Rev. B* **2015**, *91*, 195411; b) W. M. Parkin, A. Balan, L. Liang, P. M. Das, M. Lamparski, C. H. Naylor, J. A. Rodríguez-Manzo, A. T. C. Johnson, V. Meunier, M. Drndić, *ACS Nano* **2016**, *10*, 4134.
[35] Y. P. Li, A. T. Li, F. F. Li, D. P. Liu, Y. M. Chai, C. G. Liu, *J. Catal.* **2014**, *317*, 240.
[36] K. Yamamoto, T. Utsunomiya, T. Ichii, H. Sugimura, *Jpn J. Appl. Phys.* **2024**, *63*, 04SP28.
[37] W. Melitz, J. Shen, A. C. Kummel, S. Lee, *Surf. Sci. Rep.* **2011**, *66*, 1.
[38] C. Lattyak, K. Gehrke, M. Vehse, *J. Phys. Chem. C* **2022**, *126*, 13929.
[39] A. Anto Jeffery, C. Nethravathi, M. Rajamathi, *J. Phys. Chem. C* **2014**, *118*, 1386.
[40] D. Voiry, H. Yamaguchi, J. Li, R. Silva, D. C. B. Alves, T. Fujita, M. Chen, T. Asefa, V. B. Shenoy, G. Eda, M. Chhowalla, *Nat. Mater.* **2013**, *12*, 850.
[41] W. Shi, Z. Wang, Y. Q. Fu, *J. Nanoparticle Res.* **2017**, *19*, 296.
[42] J. H. Lee, W. S. Jang, S. W. Han, H. K. Baik, *Langmuir* **2014**, *30*, 9866.
[43] D. Nečas, P. Klapetek, *Open Phys.* **2012**, *10*, 181.